Dominant Factors Governing the Rate Capability of a TiO_2 Nanotube Anode for High Power Lithium Ion Batteries

Hyungkyu Han,[†,#] Taeseup Song,[†,#] Eung-Kwan Lee,[†] Anitha Devadoss,[†] Yeryung Jeon,[‡] Jaehwan Ha,[†] Yong-Chae Chung,[†] Young-Min Choi,[§] Yeon-Gil Jung,[⊥] and Ungyu Paik[†,‡,*]

[†]Department of Materials Science & Engineering and [‡]WCU Department of Energy Engineering, Hanyang University, Seoul 133-791, Korea, [§]Energy Lab, Samsung Advanced Institute of Technology, Samsung Electronics Co. Ltd., Suwon 440-600, Korea, and [⊥]School of Nano and Advanced Materials Engineering, Changwon National University, Changwon 641-773, Korea. [#]These authors contributed equally to this work.

ABSTRACT

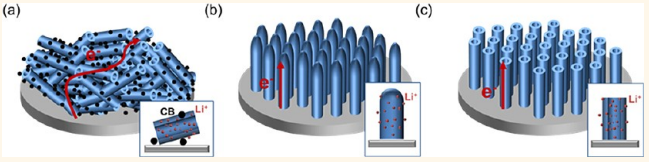

Titanium dioxide (TiO_2) is one of the most promising anode materials for lithium ion batteries due to low cost and structural stability during Li insertion/extraction. However, its poor rate capability limits its practical use. Although various approaches have been explored to overcome this problem, previous reports have mainly focused on the enhancement of both the electronic conductivity and the kinetic associated with lithium in the composite film of active material/conducting agent/binder. Here, we systematically explore the effect of the contact resistance between a current collector and a composite film of active material/conducting agent/binder on the rate capability of a TiO_2-based electrode. The vertically aligned TiO_2 nanotubes arrays, directly grown on the current collector, with sealed cap and unsealed cap, and conventional randomly oriented TiO_2 nanotubes electrodes were prepared for this study. The vertically aligned TiO_2 nanotubes array electrode with unsealed cap showed superior performance with six times higher capacity at 10 C rate compared to conventional randomly oriented TiO_2 nanotubes electrode with 10 wt % conducting agent. On the basis of the detailed experimental results and associated theoretical analysis, we demonstrate that the reduction of the contact resistance between electrode and current collector plays an important role in improving the electronic conductivity of the overall electrode system.

KEYWORDS: TiO_2 · rate capability · lithium ion batteries

Rechargeable lithium-ion batteries (LIBs) have been considered as an attractive energy storage pathway for electric vehicle (EV), plug-in hybrid electric vehicle (PHEV), and smart grid due to their lightweight, relatively high specific energy and specific power.[1,2] To successfully expand their application fields, the safety issue, one of the major problems of LIBs, should be addressed. In this context, TiO_2 is a promising anode material for LIBs due to its high working voltage (more than 1.5 V *vs* Li) and structural stability during lithium insertion/extraction,[3−5] which is free from the decomposition of organic electrolyte and short-circuit caused by the electrode swelling during cycling.[6] However, the inherent poor rate capability of TiO_2-based anode limits its practical use.[7] Various approaches have been explored to overcome this problem. Previous reports have mainly focused on the enhancement of both the electronic conductivity and the kinetics associated with lithium in the composite film of active material/conducting agent/binder. There are two general approaches to improve the electronic conductivity in the composite film of active material/conducting agent/binder. One approach is to use one-dimensional (1D) TiO_2 structures such as nanowires and nanotubes because of the ability of the efficient electron transport along its 1D geometry.[8−11] The other approach is to blend TiO_2 active material with either carbonaceous materials or other conducting metals. To improve the kinetics associated with lithium, the porous TiO_2 nanostructures were suggested. Their high interface area between active materials and the electrolyte, and the nanometer-sized dimension results in large lithium flux and short lithium diffusion length, respectively, which leads to an improvement in kinetics associated with lithium.[12,13] Although significant advancement has been achieved by engineering electrode composition and configuration, further improvement is still required.

Generally, the contact resistance between the metal and semiconducting material was carefully considered in an electronic device. A poor contact between the metal and semiconducting material results in the degradation of the electronic device.

* Address correspondence to upaik@hanyang.ac.kr.

Received for review July 5, 2012 and accepted August 30, 2012.

Published online August 30, 2012
10.1021/nn303002u

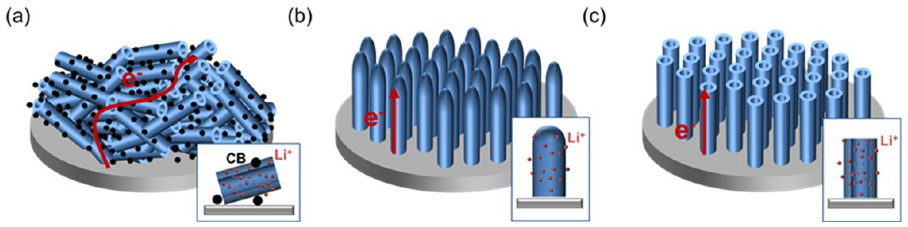

Scheme 1. Schematic illustration of randomly oriented TiO_2 nanotubes (a), directly grown sealed TiO_2 nanotube arrays (b), and unsealed TiO_2 nanotubes arrays (c) on the current collector.

Similar with the electronic device, it is expected that the electronic resistance between the current collector and the composite film of active material/conducting agent/binder in the battery system could also play an important role on the electronic conductivity of the overall electrode system since high electronic resistance at the interface could act as a huge barrier for electron injection from the current collector to the electrode. Especially, the use of electrically insulating binder and the physical contact between active material and current collector leads to significant degradation of the electronic conductivity of the overall electrode system. However, there is no systematic study of the contact resistance effect on the rate capability of TiO_2-based electrodes. Understanding the various factors governing the rate capability and engineering the materials and device system is critical to improve the performance of TiO_2-based electrodes.

Here, we present a detailed, systematic study of the contact resistance effect on the rate capability of TiO_2-based electrodes through combined experimental results and theoretical analysis. This systematic study could yield an underlying design guideline on the electrode materials for high power density LIBs. Three types of electrodes were prepared for this study. The conventional, randomly oriented TiO_2 nanotubes electrode (Scheme 1a) was prepared by mixing preformed TiO_2 nanotubes with conducting agent and binder. The vertically aligned TiO_2 nanotubes array electrodes with sealed (Scheme 1b) and unsealed caps (Scheme 1c) were directly grown on the current collector. The conventional, randomly oriented TiO_2 nanotubes electrode, as described in Scheme 1a, has physical contact and/or chemical contact with a current collector through the binder, which results in high contact resistance at the electrode/current collector interface. Although carbon conducting agent and 1D nanostructure are helpful in improving the electronic conductivity, randomly ordered geometry of the active material and the existence of many interfaces between the electrode components, such as active materials, binder, and conducting agents, could lead to longer electron pathway. Scheme 1b illustrates vertically aligned TiO_2 nanotubes array electrodes with highly ordered 1D geometry which provides short and straight electron pathways that could allow efficient electron transport in the electrode. Additionally, their direct chemical bonding with current collector could reduce the electronic resistance for electron injection from the current collector to the electrode. With an aim to explore the influence of kinetics associated with lithium on the rate capability of the TiO_2 based electrodes, the sealed cap of vertically aligned TiO_2 nanotubes array was opened. Exposing the inner surface of TiO_2 nanotubes increases the interface area between the electrolyte and active material, which could lead to large Li ion flux. Furthermore, the lithium ion diffusion length is also reduced. This specific electrode design benefits the kinetics associated with lithium in conjunction with the overall electronic conductivity of the electrode.

RESULTS AND DISCUSSION

Figure 1 presents the electron microscope images of randomly oriented TiO_2 nanotubes electrode and sealed and unsealed TiO_2 nanotubes array electrodes. The randomly oriented TiO_2 nanotubes electrode was prepared by a conventional mixing process. Vertically aligned TiO_2 nanotubes array electrodes were directly grown on the current collector using a template-assisted synthesis method.[14] Cross-sectional SEM images (Figure 1d,g) reveal the vertically aligned geometry and the existence of direct contact between the TiO_2 nanotubes array and current collector. All electrodes have identical film thickness of 2 μm (Figure 1a,d,g). The unsealed TiO_2 nanotubes array was simply obtained by opening the top-end of the sealed TiO_2 nanotubes using a reactive ion etching (RIE) method. After the RIE process, the sealed cap was opened (Figure 1g,h), and the vertically aligned morphology was retained without any structural damages like cracking or crumbling. Low magnification TEM images reveal that TiO_2 nanotubes in all cases have the outer diameter of 100 nm and the wall thickness of 20 nm, respectively. High resolution TEM images and selective area electron diffraction (SAED) patterns (insets of Figure 1 images c, f, and i) depict that the TiO_2 nanotubes have an anatase phase, which is consistent with XRD results (Supporting Information, Figure S1). A lattice spacing of 3.5 Å corresponds to the (101) planes of anatase TiO_2.[15] The polycrystalline TiO_2 nanotube has the conductivity value of 8×10^{-6} S·cm^{-1}, which is comparable to those of typical polycrystalline TiO_2 anatase films.[16,17] (Supporting Information, Figure S10)

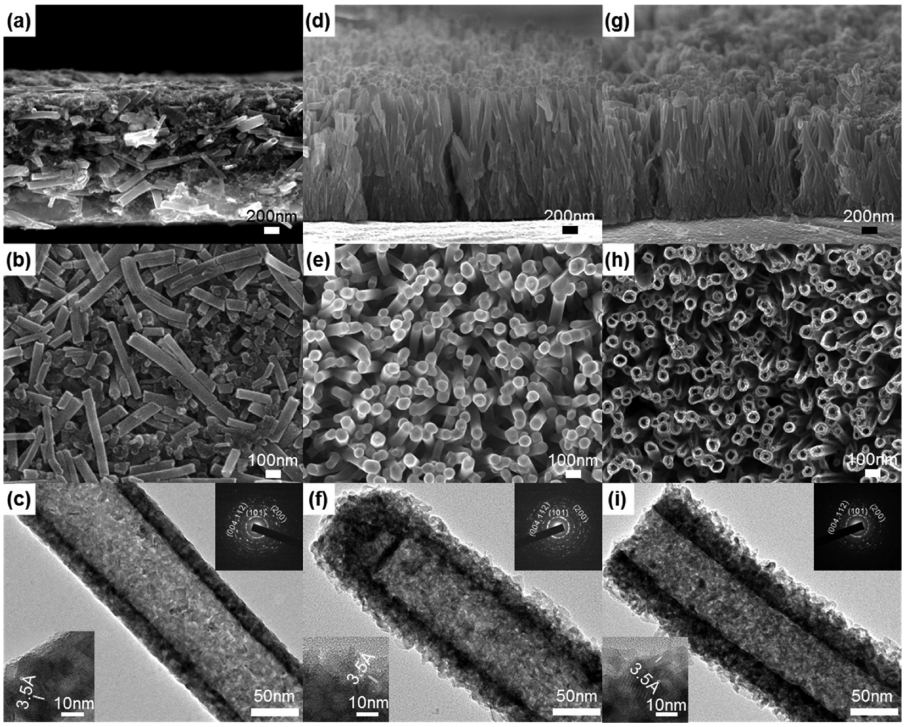

Figure 1. Cross sectional, top-view SEM images and TEM image of randomly oriented (a−c), directly grown sealed (d−f), and unsealed (g−i) TiO_2 nanotubes on the current collector, respectively. Right-up and left-down insets in images c, f, and i show the corresponding selective area electron diffraction patterns and HR-TEM images, respectively.

Figure 2 shows the voltage profiles at the first cycle and cyclic performances for sealed and unsealed TiO_2 nanotubes array electrodes and randomly oriented TiO_2 nanotubes electrodes with various carbon black amounts (10, 20, and 30 wt %). Their electrochemical performances were evaluated in the voltage range 1−3 V *vs* Li/Li^+ at a rate of 0.2 C. All electrodes exhibit a typical voltage profile of an anatase type TiO_2 anode.[18] The voltage plateaus around 1.73 and 1.88 V correspond to lithium intercalation into and deintercalation from the interstitial octahedral sites of anatase TiO_2, respectively.[19] The sealed and unsealed TiO_2 nanotubes array electrodes exhibit charge capacities of 213.5 and 214.3 mAh/g and discharge capacities of 191.9 and 193.8 mAh/g, which indicate the Coulombic efficiency of 89.9 and 90.4%, respectively. It is well-known that the Coulombic efficiency decreases with surface area of the active materials due to an increase in the formation of solid-electrolyte interface (SEI), which is closely related to irreversible capacity.[20] Since the SEI layer is not formed on the TiO_2 materials due to its high working voltage, an unsealed TiO_2 nanotubes array electrode could show similar Coulombic efficiency compared to that of a sealed TiO_2 nanotubes array electrode.[19] The conventional randomly oriented TiO_2 nanotubes electrode shows comparatively lower charge capacity and initial Coulombic efficiency than those of sealed and unsealed TiO_2 nanotube array electrodes. The role of conducting agent amount on the charge/discharge capacities is negligible at low current rate (0.2 C). The origin for the irreversible capacity in TiO_2 electrodes is not yet clearly understood. The suggested possible origins for the irreversible capacity of TiO_2 electrodes in the first cycle are (i) lithium intercalation into irreversible sites,[21] (ii) side reaction caused by the water absorbed on TiO_2 electrode,[22] and (iii) poor intrinsic electronic conductivity of TiO_2.[23] Further study needs to be carried out to clarify this point. Detailed values of charge, discharge capacities, and Coulombic efficiencies for these electrodes are summarized in Supporting Information, Table S1. The cycle performances were also evaluated (Figure 2b). All electrodes show excellent cycle performances without any noticeable capacity fading and exhibit high Coulombic efficiency over 99% after 10 cycles. The morphological changes for all electrodes after 100 cycles were observed (Supporting Information, Figure S2). Both the sealed and unsealed TiO_2 nanotubes array electrodes exhibit identical morphologies with those of pristine TiO_2 nanotubes array electrodes and maintain the directly grown configuration without delaminating from the current collectors. Randomly oriented TiO_2 nanotubes electrodes also maintain their initial morphology regardless of the amount of conducting agent.

Figure 3 shows the discharge capacities of sealed and unsealed TiO_2 nanotubes array electrodes and randomly oriented TiO_2 nanotubes electrodes with various carbon black amounts (10, 20, and 30 wt %) at various current rates. It is clearly observed that the

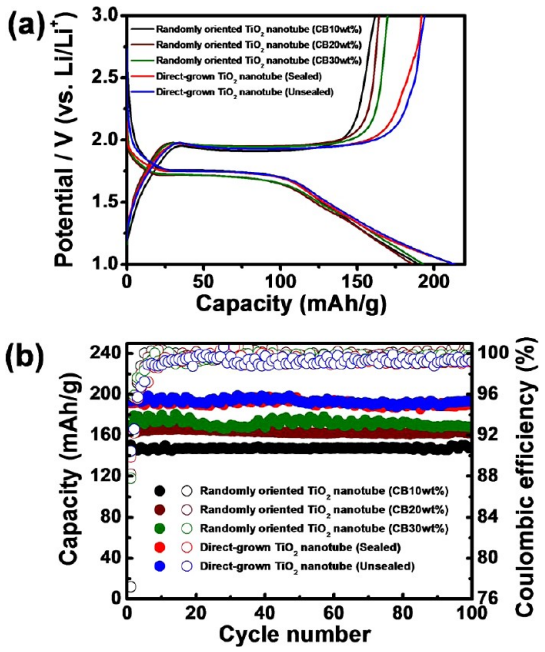

Figure 2. Electrochemical characteristics of sealed and unsealed TiO_2 nanotubes electrodes directly grown on a current collector and randomly oriented TiO_2 nanotubes electrodes with various amounts of carbon black (10 to 30 wt %): (a) Voltage profiles at the first cycle; (b) cycle performances at a rate of 0.2 C (closed circle, specific capacity; and open circle, Coulombic efficiency).

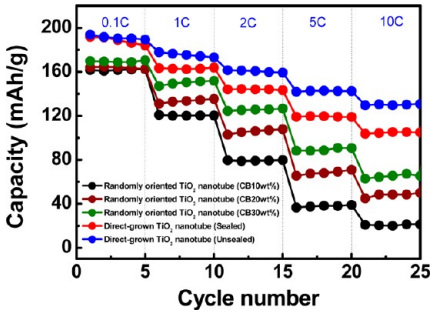

Figure 3. Specific capacities of sealed and unsealed TiO_2 nanotubes electrodes directly grown on a current collector and randomly oriented TiO_2 nanotubes electrodes with various amounts of carbon black (10 to 30 wt %) at different current densities.

discharge capacity of randomly oriented TiO_2 nanotubes electrode increases with the amount of conducting agent specifically at higher current rates. Briefly, randomly oriented TiO_2 nanotubes electrodes with 10, 20, and 30 wt % conducting agent deliver the discharge capacities of 20.9, 48.1, and 65.1 mAh/g at a current density 10 C, respectively. The enhancement of electronic conductivity in composite film of active material/conducting agent/binder enables an improvement in rate capability of TiO_2-based electrode. On the other hand, sealed and unsealed TiO_2 nanotubes array electrodes exhibit much improved rate capabilities even in the absence of a conducting agent compared to that of a randomly oriented TiO_2 nanotubes electrode with 30 wt % carbon black. Especially, an unsealed TiO_2 nanotubes array electrode showed comparable or improved electrochemical performances compared to previously reported impressive results of TiO_2-based anode materials without any conductive agent. An unsealed TiO_2 nanotubes array electrode delivered the capacity over about 130 mAh/g at the 10 C rate. An anatase TiO_2 nanosheet hierarchical spheres electrode (TiO_2 sphere/conductive agent/binder = 70:20:10),[24] TiO_2-graphene sheets hybrid electrode (TiO_2-graphene sheets/conductive agent/binder = 80:10:10)[25] and TiO_2 nanonetwork electrode (TiO_2 nanonetwork/conductive agent/binder = 66:26:8)[8] showed discharge capacities of 125, 125, and 90 mAh/g at 10, 10, and 5 C rate, respectively. These results strongly suggest that the electrode configuration having direct contact between the current collector and the active material plays a more important role on an improvement in the rate capability compared to the enhancement of electronic conductivity in the composite film of active material/conducting agent/binder, as discussed in a theoretical analysis described subsequently. It should be noted that the sealed and unsealed TiO_2 nanotubes array electrodes have much higher area and volume capacities compared to those of randomly oriented TiO_2 nanotubes electrode, especially at the high current rate, due to both their densely packed geometries and the absence of conducting agent and binder. (Supporting Information, Table S3) This is a striking feature addressing the problems associated with the low energy density of TiO_2 anode, which is another problem on its practical use. The unsealed TiO_2 nanotubes array electrode shows slightly improved rate capability compared to that of sealed TiO_2 nanotubes array. This result came from more favorable Li related kinetics caused by geometrical advantages of unsealed hollow morphology, which was well described in our previous report.[26] On the basis of the above comparative study, we could conclude that the dominant factor governing rate capability of TiO_2-based electrodes is electronic property, especially the resistance between the electrode and current collector, in the overall electrode system.

AC impedance analysis for the half cell was carried out to further elucidate the influence of the contact resistance at the active material/current collector interface on cell performance. The half cells were fabricated using randomly oriented TiO_2 nanotubes mixed with different amounts of conducting agents and directly grown TiO_2 nanotube arrays on the current collector. The resulting impedance Nyquist spectra of all electrodes are presented in Figure 4. An equivalent circuit[27,28] (inset of Figure 4) was used to analyze the electronic interfacial parameters of the cells, and the resultant values are enlisted in Supporting Information, Table S2. As shown in Figure 4, the randomly oriented TiO_2 nanotubes electrode shows a depressed semicircle ranging from high to medium frequency. It is well-known

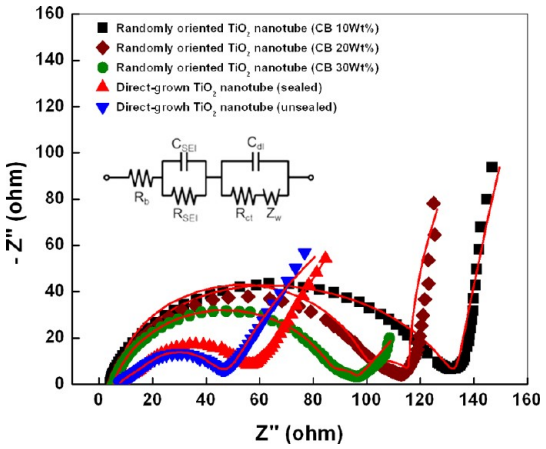

Figure 4. Nyquist plots of different anode configurations including randomly oriented TiO_2 nanotubes with carbon black (10 to 30 wt %), sealed and unsealed TiO_2 nanotubes directly grown on a current collector. The filled circles in the spectra represent experimental data, whereas the solid lines represent fitting curve. The inset shows the equivalent circuit.

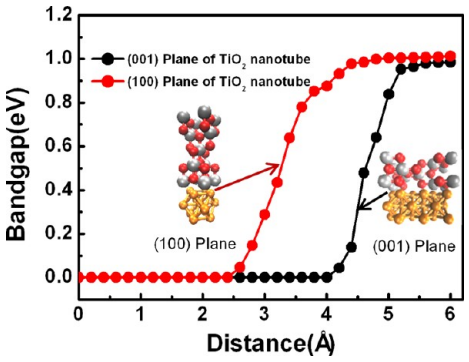

Figure 5. Plot of the band gap energy change of Ti based on the separation between TiO_2 anatase surface and Cu (001) substrate from the equilibrium junction structure. The black and red dots represent the calculated energy from the interface between the Cu (001) substrate and TiO_2 anatase (001) and (100) surface, respectively. The silver, red, and orange spheres represent Ti, O, and Cu atoms, respectively.

that the shape of the impedance arc (depressed or distinct) relies on the contact impedance between the electrode material and the current collector.[29] Thus, we expect that the assembling modes of TiO_2 nanotubes on the current collector greatly control the contact resistance and play a crucial role in cell performance. In the case of randomly oriented TiO_2 nanotubes electrode, the contact resistance shows strong dependence on the amount of carbon black due to the variation in the surface coverage of the conductive agents on the TiO_2 nanotubes. At lower amounts of carbon black, poor electrical contact that could impede the electron flow from collector to the active materials is formed between the current collector and the active materials.[30,31] This apparently increases the contact resistance of the cells which increases the overall surface resistance to ~127 Ω. The R_{semi} for higher carbon additive (30 wt %) is found to be ~89.8 Ω. However, excessive addition of carbon black into the electrode composite results in a significant decrease in area and volume capacities. In striking contrast, the directly grown TiO_2 nanotubes electrode showed much smaller resistance (55.7 Ω) than those of the randomly oriented TiO_2 nanotubes electrodes (89.8 Ω) even without the presence of additional conductive agents. The high accessibility of electron conduction from enriched electrical contacts at the current collector decreases the contact resistance at the electrode material/current collector interface.[32] Furthermore, the unsealed TiO_2 nanotubes array electrode exhibits the lowest R_{ct} value (43.4 Ω). The R_{ct} is the whole resistance (charge transfer resistance at TiO_2 anode surface and contact resistance at collector). As both sealed and unsealed TiO_2 nanotubes arrays have similar contact resistance, the difference in R_{ct} values between these samples is attributed to charge transfer resistance at the TiO_2 anode surface. The unsealed TiO_2 nanotube provides an additional interface area between the electrolyte and the active material, which allows larger lithium-ion flux and shorter diffusion distance of the lithium ions compared to those of the sealed TiO_2 nanotube. These advantages related to Li kinetics for the unsealed TiO_2 nanotube result in improvement in charge transfer and decrease in R_{ct} value. From the above discussion, the less surface resistance components supported by the directly grown anode architecture enable the improvement in the rate capability of the cell (Figure 3). In this study, we prepared TiO_2 nanotubes electrodes with identical film thickness of about 2 μm and evaluated their electrochemical performances. For the practical use, the thickness of the electrode should be much increased to achieve high energy density. As shown in Supporting Information, Figure S10, the electronic resistance of the TiO_2 electrode increases with the length of TiO_2 nanotubes on the current collector, which leads to the deterioration in the electrochemical performances. This problem could be addressed by improving the electronic conductivity of TiO_2 active materials. Many approaches have been explored to improve the electronic conductivity of the TiO_2. The most efficient method is the introduction of a highly conducting layer, such as carbon layer[33] or TiN/TiO_xN_y layer[34] on the surface of the TiO_2. Further improvement in rate capability for the TiO_2-based electrode could be achieved by combining the electrode configuration with direct contact to the current collector, presented here, and an introduction of a highly conducting layer on the surface of the TiO_2 active material regardless of the thickness of the electrode. Further study will be carried out to clarify this point.

Theoretical analysis provides an insight into the underlying physics of electronic resistance between the electrode and current collector in both the vertically aligned TiO_2 nanotubes array electrodes and the randomly oriented TiO_2 nanotubes electrode (Figure 5). Both vertically aligned and randomly oriented TiO_2

nanotubes electrodes have chemical and physical contact with the current collector, respectively. The bonding distance between the TiO_2 nanotubes and current collector is the key parameter determining the electronic resistance between the electrode and current collector since the 3d-state of Ti is changed by the Cu substrate when their bonding distance gets closer. The density functional theory (DFT) was applied to quantitatively and theoretically study the electronic structure change as a function of the bonding distance between TiO_2 nanotubes and metal substrate. As shown in Figure 5, the band gap energy was calculated as a function of the distance between the TiO_2 nanotubes and Cu (001) substrate from the equilibrium junction structures. The band gap energy was obtained from the density of states (DOS) . DOS is determined using the following equation:

$$\bar{n}(\varepsilon_i) = (N(\varepsilon_i) - N(\varepsilon_{i-1}))/\Delta\varepsilon$$

where, ε_i is the ith energy state, $\Delta\varepsilon$ is the distance between the two nearest energy states, and $N(\varepsilon_i)$ is the integrated DOS. $N(\varepsilon_i)$ is defined as follows:

$$N(\varepsilon_i) = \int_{-\infty}^{\varepsilon_i} n(\varepsilon)\, d\varepsilon$$

As shown in Figure 1c,f, vertically aligned TiO_2 nanotubes array electrodes have a polycrystalline anatase phase. Therefore, we mainly considered both (001) and (100) surfaces of TiO_2, since these surfaces have the lowest surface energy. Chemically bonded Ti in each direction exhibits the metallic characteristic since its Fermi level is located on the conduction band. (Figure 5) However, as the separations of TiO_2 anatase (001) and (100) surface with Cu (001) substrate are over 4.0 and 2.4 Å, respectively, the band gap energy of Ti grows larger. The band gap energy that converges at 1.0 eV around the physical bonding region is ~5.0 Å. This shows that the electronic characteristics of Ti on the interface change from metallic to semiconducting by band gap formation. Therefore, chemically bonded arrayed structures (Figure 1b,c) display superior conduction properties than physically bonded randomly oriented structures (Figure 1a).

CONCLUSION

We have explored the role of key factors governing the rate capability of TiO_2-based electrodes through the systematic approach by fabricating sealed and unsealed TiO_2 nanotubes arrays and randomly oriented nanotubes electrodes. Both the experimental results and theoretical analysis proved that a TiO_2 nanotubes array grown directly on a current collector showed superior rate capability than conventional randomly oriented electrodes. This result suggests that the resistance between the electrode and current collector plays a major role on the rate capabilities of TiO_2based electrodes, despite achieving improved kinetics and electronic conductivity in the composite film. Our systematic analysis offers significant insight into the factors controlling the device performance of LIBs.

EXPERIMENTAL SECTION

Preparation of TiO_2 Hollow Nanofibers. Titanium tetraisopropoxide ($Ti(OiPr)_4$, Aldrich, 3 g) was mixed with acetic acid (2 mL) and ethanol (2 mL). After 10 min, this solution was added to ethanol (3 mL) that contains polyvinyl pyrrolidone (PVP) (Aldrich, $M_w \approx$ 1 300 000, Aldrich, 0.3 g). The prepared solutions were mixed using a magnetic stirrer for 20 min and immediately loaded into a plastic syringe connected to the metallic outer needle, and heavy mineral oil (Aldrich) was added to another syringe connected to the metallic inner needle. The feeding rates of PVP solution and mineral oil were set at 0.6 mL/h and 0.2 mL/h, respectively. This dual nozzle was connected to a high-voltage supply, and aluminum foil was placed 12 cm below the tip of the needle to collect the nanofibers. The electrospinning process was conducted in air. The as-spun nanofibers were left in air for ~5 h to allow the hydrolysis of $Ti(OiPr)_4$ to complete. The mineral oil was extracted by immersing the fibers in octane overnight. Finally, hollow nanofibers were obtained by calcining them in air at 500 °C for 1 h.

Preparation of Sealed TiO_2 Nanotube Arrays on the Metallic Current Collector. A thin ZnO seed layer was deposited on the current collector with 15 mm diameter by radio frequency magnetron sputtering. Arrays of ZnO nanorods, which serve as sacrificial templates for the nanotubes, were grown on the seed layer by a hydrothermal method at 85 °C for 10 h. Zinc nitrate hexahydrate (0.025 M) and hexamethylentetramine (0.025 M) were used as precursor chemicals. The synthesized ZnO nanorod arrays on the current collector were immersed in an aqueous solution consisting of 0.075 M ammonium hexafluorotitanate and 0.2 M boric acid at room temperature for 0.5 h. In this solution, ammonium hexafluorotitanate hydrolyzed to TiO_2 on the individual ZnO nanorod while ZnO dissolved simultaneously in the solution with acids produced by ammonium hexafluorotitanate hydrolysis. Subsequently, the resulting TiO_2 nanotube arrays immersed in a 0.5 M boric acid solution for 1 h to remove the residual ZnO inside the tubes. The arrays were finally rinsed with DI water and calcined in Ar at 500 °C for 0.5 h to increase crystallinity.

Preparation of Unsealed TiO_2 Nanotube Arrays on the Metallic Current Collector. The resulting sealed TiO_2 nanotube arrays were etched by RIE with a 120 sccm carbon fluoride gas at 100 W for 1 min.

Characterization. The sealed and unsealed TiO_2 nanotube arrays on the current collector and as-prepared TiO_2 hollow nanofibers were characterized using a field emission scanning electron microscope (FE-SEM, JEOL JSM-7600F), a field emission transmission electron microscope (FE-TEM, JEOL JEM-2100F), high-resolution transmission electron microscopy (HRTEM, JEOL JEM-2100F), advanced potentiostat (Princeton Applied Research PARSTAT 2273), and X-ray diffraction (XRD, Rigaku D/MAX RINT-2000).

Characterization of the Electrical Properties of TiO_2 Nanotube Arrays. To characterize the electrical properties of TiO_2 nanotubes directly grown on the current collector, the vertically aligned TiO_2 nanotubes arrays with different length were synthesized. (Supporting Information, Figure S8) The free space between the TiO_2 nanotubes was filled with polymer resin. The tip of TiO_2 nanotubes array was exposed using O_2 plasma, and then patterned Cu thin film (600 μm × 600 μm) was deposited on the tip of TiO_2 nanotubes array using a thermal evaporator. The schematic illustration and corresponding SEM images for the experimental process are presented in Supporting Information, Figure S9. The conductivity of the TiO_2 nanotube was obtained based on $I-V$ characteristic results and the theoretical calculation. The contact resistance of the TiO_2 nanotube with the current collector was obtained from Supporting Information, Figure S10.

Evaluation of Electrochemical Properties. The sealed and unsealed TiO_2 nanotube arrays on the current collector acts as anode. The randomly oriented TiO_2 nanotube electrodes were fabricated using TiO_2 hollow nanofiber powders as the active materials combined with conductive carbon blacks and polyvinylidene fluoride (PVDF) binder in a weight ratio of 80:10:10, 70:20:10, 60:30:10, respectively. The slurry was coated on a copper foil and dried overnight in a vacuum oven at 100 °C. Coin-type half cells (2016R type) were fabricated to evaluate the electrochemical properties of all types of the TiO_2 as working electrodes. Pure lithium metal foil was used as the counter-electrode. One M $LiPF_6$ in ethylene carbonate/diethylene carbonate (EC/DEC, 1:1 vol %, PANAX StarLyte, S. Korea) was used as the electrolyte. The coin-type half cells were cycled at a rate of 0.2 C between 1 and 3 V using a battery cycle tester (TOSCAT 3000, Toyo Systems, Tokyo, Japan). All TiO_2 nanotube electrodes showed high reproducibility without noticeable sample-to-sample variation (Supporting Information, Figures S3−S7, Table S4)

Theoretical Analysis. The DFT calculations to determine the band gap energy of TiO_2 anatase on Cu (001) surface was performed using the VASP code.[35] For the modeling of TiO_2 anatase and Cu interface, the single layer of TiO_2 anatase slabs were cut in the [100] and [001] crystallographic directions and were located on the $1 \times 1 \times 3$ and $3 \times 1 \times 3$ Cu (001) surfaces, respectively. The plane-wave basis set was set to a cutoff energy of 300 eV. The $8 \times 8 \times 1$ and $1 \times 8 \times 1$ *k*-point grids generated by the Monkhorst−Pack scheme were used for the structural relaxations and the band gap energy calculations of the single TiO_2 anatase (001) and (100) surface on the Cu (001) substrate, respectively.[36] The projector-augmented waves (PAW) and the generalized gradient approximation (GGA) were used.[37,38] Since another Cu/TiO_2 anatase interface, which has same structure with TiO_2 anatase/Cu interface, was made by the periodic boundary system, vacuums were inserted to both interfaces to reflect the separation between the TiO_2 anatase surface and the Cu substrate.

Conflict of Interest: The authors declare no competing financial interest.

Acknowledgment. This work was financially supported by the National Research Foundation of Korea (NRF) through Grant No. K20704000003TA050000310, Global Research Laboratory (GRL) Program provided by the Korean Ministry of Education, Science and Technology (MEST) in 2011, the International Cooperation program of the Korea Insitute of Energy Technology Evaluation and Planning(KETEP) grant funded by the Korea Ministry of Knowledge Economy (No. 2011T100100369), and WCU (World Class University) program through the National Research Foundation of Korea funded by the Ministry of Education, Science and Technology (R31-10092).

Supporting Information Available: Tables S1−S4 and Figures S1−S10 as described in the text. This material is available free of charge via the Internet at http://pubs.acs.org.

REFERENCES AND NOTES

1. Gratzel, M. Photoelectrochemical Cells. *Nature* **2001**, *414*, 338–344.
2. Bruce, P. G.; Scrosati, B.; Tarascon, J. M. Nanomaterials for Rechargeable Lithium Batteries. *Angew. Chem., Int. Ed.* **2008**, *47*, 2930–2946.
3. Liu, S.; Pan, G. L.; Yan, N. F.; Gao, X. P. Aqueous TiO_2/$NiOH_2$ Rechargeable Battery with a High Voltage Based on Proton and Lithium Insertion/Extraction Reactions. *Energy Environ. Sci.* **2010**, *3*, 1732–1735.
4. Subramanian, V.; Karki, A.; Gnanasekar, K. I.; Eddy, F. P.; Rambabu, B. Nanocrystalline TiO_2 (Anatase) for Li-Ion Batteries. *J. Power Sources* **2006**, *159*, 186–192.
5. Olson, C. L.; Nelson, J.; Islam, M. S. Defect Chemistry, Surface, and Lithium Insertion in Anatase TiO_2. *J. Phys. Chem. B* **2006**, *110*, 9995–10001.
6. Huang, S. Y.; Kavan, L.; Exnar, I.; Gratzel, M. Rocking Chair Lithium Battery Based on Nanocrystalline TiO_2 (Anatase). *J. Electrochem. Soc.* **1995**, *142*, L142–L144.
7. Arico, A. S.; Bruce, P.; Scrosati, B.; Tarascon, J. M.; Van Schalkwijk, W. Nanostructured Materials for Advanced Energy Conversion and Storage Devices. *Nat. Mater.* **2005**, *4*, 366–377.
8. Kim, S. W.; Han, T. H.; Kim, J.; Gwon, H.; Moon, H. S.; Kang, S. W.; Kim, S. O.; Kang, K. Fabrication and Electrochemical Characterization of TiO_2 Three-Dimensional Nanonetwork Based on Peptide Assembly. *ACS Nano* **2009**, *3*, 1085–1090.
9. Wu, F. X.; Wang, Z. X.; Li, X. H.; Guo, H. J. Hydrogen Titanate and TiO_2 Nanowires as Anode Materials for Lithium-Ion Batteries. *J. Mater. Chem.* **2011**, *21*, 12675–12681.
10. Wu, H. B.; Hng, H. H.; Lou, X. W. Direct Synthesis of Anatase TiO_2 Nanowires with Enhanced Photocatalytic Activity. *Adv. Mater.* **2012**, *24*, 2567–2571.
11. Li, J. M.; Wan, W.; Zhou, H. H.; Li, J. J.; Xu, D. S. Hydrothermal Synthesis of TiO_2(B) Nanowires with Ultrahigh Surface Area and Their Fast Charging and Discharging Properties in Li-Ion Batteries. *Chem. Commun.* **2011**, *47*, 3439–3441.
12. Hu, Y. S.; Kienle, L.; Guo, Y. G.; Maier, J. High Lithium Electroactivity of Nanometer-Sized Rutile TiO_2. *Adv. Mater.* **2006**, *18*, 1421–1426.
13. Hassoun, J.; Panero, S.; Simon, P.; Taberna, P. L.; Scrosati, B. High-Rate, Long-Life Ni−Sn Nanostructured Electrodes for Lithium-Ion Batteries. *Adv. Mater.* **2007**, *19*, 1632–1635.
14. Xu, C. K.; Shin, P. H.; Cao, L. L.; Wu, J. M.; Gao, D. Ordered TiO_2 Nanotube Arrays on Transparent Conductive Oxide for Dye-Sensitized Solar Cells. *Chem. Mater.* **2010**, *22*, 143–148.
15. Dai, Y. Q.; Cobley, C. M.; Zeng, J.; Sun, Y. M.; Xia, Y. N. Synthesis of Anatase TiO_2 Nanocrystals with Exposed {001} Facets. *Nano Lett.* **2009**, *9*, 2455–2459.
16. Akl, A. A.; Kamal, H.; Abdel-Hady, K. Fabrication and Characterization of Sputtered Titanium Dioxide Films. *Appl. Surf. Sci.* **2006**, *252*, 8651–8656.
17. Huber, B.; Gnaser, H.; Ziegler, C. Electrical Properties of Nanocrystalline Anatase TiO_2 Thin Films with Different Crystallite Size. *Surf. Sci.* **2004**, *566*, 419–424.
18. Kim, J.; Cho, J. Rate Characteristics of Anatase TiO_2 Nanotubes and Nanorods for Lithium Battery Anode Materials at Room Temperature. *J. Electrochem. Soc.* **2007**, *154*, A542–A546.
19. Deng, D.; Kim, M. G.; Lee, J. Y.; Cho, J. Green Energy Storage Materials: Nanostructured TiO_2 and Sn-Based Anodes for Lithium-Ion Batteries. *Energy Environ. Sci.* **2009**, *2*, 818–837.
20. Graetz, J.; Ahn, C. C.; Yazami, R.; Fultz, B. Highly Reversible Lithium Storage in Nanostructured Silicon. *Electrochem. Solid-State Lett.* **2003**, *6*, A194–A197.
21. Xu, J. W.; Wang, Y. F.; Li, Z. H.; Zhang, W. Preparation and Electrochemical Properties of Carbon-Doped TiO_2 Nanotubes as an Anode Material for Lithium-Ion Batteries. *J. Power Sources* **2008**, *175*, 903–908.
22. Li, J. R.; Tang, Z. L.; Zhang, Z. T. Preparation and Novel Lithium Intercalation Properties of Titanium Oxide Nanotubes. *Electrochem. Solid-State Lett.* **2005**, *8*, A316–A319.
23. Armstrong, A. R.; Armstrong, G.; Canales, J.; Bruce, P. G. TiO_2-B Nanowires as Negative Electrodes for Rechargeable Lithium Batteries. *J. Power Sources* **2005**, *146*, 501–506.
24. Chen, J. S.; Tan, Y. L.; Li, C. M.; Cheah, Y. L.; Luan, D. Y.; Madhavi, S.; Boey, F. Y. C.; Archer, L. A.; Lou, X. W. Constructing Hierarchical Spheres from Large Ultrathin Anatase TiO_2 Nanosheets with Nearly 100% Exposed (001) Facets for Fast Reversible Lithium Storage. *J. Am. Chem. Soc.* **2010**, *132*, 6124–6130.
25. Wang, D. H.; Choi, D. W.; Li, J.; Yang, Z. G.; Nie, Z. M.; Kou, R.; Hu, D. H.; Wang, C. M.; Saraf, L. V.; Zhang, J. G.; *et al.* Self-Assembled TiO_2-Graphene Hybrid Nanostructures for Enhanced Li-Ion Insertion. *ACS Nano* **2009**, *3*, 907–914.
26. Song, T.; Xia, J.; Lee, J.-H.; Lee, D. H.; Kwon, M.-S.; Choi, J.-M.; Wu, J.; Doo, S. K.; Chang, H.; Park, W. I.; *et al.* Arrays of Sealed Silicon Nanotubes as Anodes for Lithium Ion Batteries. *Nano Lett.* **2010**, *10*, 1710–1716.
27. Fabregat-Santiago, F.; Barea, E. M.; Bisquert, J.; Mor, G. K.; Shankar, K.; Grimes, C. A. High Carrier Density and Capacitance in TiO_2 Nanotube Arrays Induced by Electrochemical Doping. *J. Am. Chem. Soc.* **2008**, *130*, 11312–11316.

28. Ho, C.; Raistrick, I. D.; Huggins, R. A. Application of AC Techniques to the Study of Lithium Diffusion in Tungsten Trioxide Thin-Films. *J. Electrochem. Soc.* **1980**, *127*, 343–350.
29. Gaberscek, M.; Moskon, J.; Erjavec, B.; Dominko, R.; Jamnik, J. The Importance of Interphase Contacts in Li Ion Electrodes: The Meaning of the High-Frequency Impedance Arc. *Electrochem. Solid-State Lett.* **2008**, *11*, A170–A174.
30. Moriguchi, I.; Hidaka, R.; Yamada, H.; Kudo, T.; Murakami, H.; Nakashima, N. A Mesoporous Nanocomposite of TiO_2 and Carbon Nanotubes as a High-Rate Li-Intercalation Electrode Material. *Adv. Mater.* **2006**, *18*, 69–73.
31. Choi, M. G.; Lee, Y. G.; Song, S. W.; Kim, K. M. Anode Properties of Titanium Oxide Nanotube and Graphite Composites for Lithium-Ion Batteries. *J. Power Sources* **2010**, *195*, 8289–8296.
32. Ruffo, R.; Hong, S. S.; Chan, C. K.; Huggins, R. A.; Cui, Y. Impedance Analysis of Silicon Nanowire Lithium Ion Battery Anodes. *J. Phys.Chem. C* **2009**, *113*, 11390–11398.
33. Park, S. J.; Kim, Y. J.; Lee, H. Synthesis of Carbon-Coated TiO_2 Nanotubes for High-Power Lithium-Ion Batteries. *J. Power Sources* **2011**, *196*, 5133–5137.
34. Han, H.; Song, T.; Bae, J. Y.; Nazar, L. F.; Kim, H.; Paik, U. Nitridated TiO_2 Hollow Nanofibers as an Anode Material for High Power Lithium Ion Batteries. *Energy Environ. Sci.* **2011**, *4*, 4532–4536.
35. Kresse, G.; Furthmuller, J. Efficient Iterative Schemes for *ab Initio* Total-Energy Calculations Using a Plane-Wave Basis Set. *Phys. Rev. B* **1996**, *54*, 11169–11186.
36. Monkhorst, H. J.; Pack, J. D. Special Points for Brillouin-Zone Integrations. *Phys. Rev. B* **1976**, *13*, 5188–5192.
37. Kresse, G.; Joubert, D. From Ultrasoft Pseudopotentials to the Projector Augmented-Wave Method. *Phys. Rev. B* **1999**, *59*, 1758–1775.
38. Perdew, J. P.; Chevary, J. A.; Vosko, S. H.; Jackson, K. A.; Pederson, M. R.; Singh, D. J.; Fiolhais, C. Atoms, Molecules, Solids, and Surfaces—Applications of the Generalized Gradient Approximation for Exchange and Correlation. *Phys. Rev. B* **1992**, *46*, 6671–6687.